PHYSICAL REVIEW A VOLUME 17, NUMBER 2 FEBRUARY 1978

Single-electron capture by multiply charged ions of carbon, nitrogen, and oxygen in atomic and molecular hydrogen

R. A. Phaneuf and F. W. Meyer
Oak Ridge National Laboratory, Oak Ridge, Tennessee 37830

R. H. McKnight
University of Virginia, Charlottesville, Virginia 22901
(Received 1 August 1977)

Cross sections for electron capture by N^{+q}, O^{+q} ($1 \leq q \leq 5$), and C^{+q} ($1 \leq q \leq 4$) incident on atomic and molecular hydrogen have been measured in the velocity range $(0.3\text{–}5.2) \times 10^8$ cm/s. The capture cross sections for the higher incident charge states are large, in many cases exceeding 1×10^{-15} cm^2. For relative velocities above the Bohr velocity, all the measured cross sections were found to decrease monotonically with increasing velocity and to scale in magnitude roughly as q^2. Furthermore, for these higher velocities the cross sections for electron capture from H_2 are systematically larger than the corresponding cross sections for electron capture from H. For relative velocities below the Bohr velocity, no simple behavior of the measured cross sections was observed. The behavior of the cross sections at low velocities is discussed qualitatively using the Landau-Zener formalism. For higher velocities reasonable agreement was found with the classical trajectory Monte Carlo calculations of Olson and Salop.

I. INTRODUCTION

Electron transfer is the dominant inelastic atomic process in many physical systems and has therefore been studied extensively over the years. Numerous collision pairs have been examined, with bombarding energies ranging from thermal to many MeV. Most work has involved singly or doubly charged light-ion projectiles bombarding targets of molecular or rare gases. A small but increasing number of measurements have been made using atomic-hydrogen targets.

Until recently, investigations involving multiply charged ions have been limited to ions with velocities significantly greater than the Bohr velocity.[1] With the development of ion sources designed specifically to produce multiply charged ions, charge transfer processes can now be studied for a wide range of projectile charge states and energies.[2,3]

Such studies are of considerable interest for their intrinsic value in furthering the understanding of charge transfer mechanisms as well as for their potential application in various areas of technology. For example, collisions between multiply charged impurity ions and deuterium or hydrogen atoms in plasmas can result in energy and particle loss from the plasma and are thus important to the magnetically confined fusion program.[3] In addition, charge transfer plays a significant role in the present scheme of heating prototype tokamak fusion devices to ignition temperature by the injection of neutral hydrogen or deuterium beams. One potential source of difficulty in this scheme is charge transfer or stripping of the injected beam in collisions with multiply charged impurity ions near the plasma boundary. Collision of the resultant fast ions with the vessel walls can liberate further impurities, resulting in significant plasma cooling and the initiation of instabilities.[4] Charge transfer cross sections pertaining to this situation can be measured by bombarding an atomic-hydrogen target with multiply charged ions having the velocity of the injection beam.

Progress in theoretical work describing charge transfer processes has lagged somewhat behind the experimental effort. *Ab initio* calculations are difficult, since extensive basis sets are necessary to adequately describe the simplest charge transfer processes.[5] For certain types of nonresonant collisions, however, less detailed calculations involving a Landau-Zener formulation or two-state approximations have proven useful at low velocities.[6]

The present work has been undertaken to provide a comprehensive set of measurements of single-electron charge transfer cross sections for different charge states of nitrogen, oxygen, and carbon ($N^{+q}, O^{+q}, 1 \leq q \leq 5$, and $C^{+q}, 1 \leq q \leq 4$) bombarding atomic- and molecular-hydrogen target gases. In addition to having applicability to the neutral beam injection problem, these results should prove useful for testing various theoretical calculations of charge transfer processes involving multiply charged ions.

II. EXPERIMENTAL METHOD

A. General description

Carbon, nitrogen, and oxygen ions of charge +1, +2, and +3 were produced in an electron-bombard-

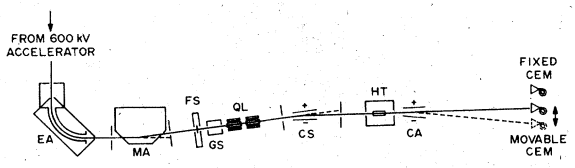

FIG. 1. Schematic diagram of the apparatus. EA, electrostatic analyzer; MA, magnetic analyzer; FS, foil stripper; GS, gas stripper; QL, electrostatic quadrupole lens; CS, electrostatic charge selector plates; HT, hydrogen target oven; CA, electrostatic charge analyzer plates; CEM, channel electron multiplier.

ment source which was part of a conventional 600-keV accelerator. After acceleration, the ions were electrostatically deflected through 90° and their momentum was analyzed by bending through 8° with a magnet. A schematic of the experimental apparatus is shown in Fig. 1. Ions of higher charge states were produced by passing a selected beam through a gas cell or a thin formvar foil. After stripping, a given charge state was selected by deflection plates CS and was directed into the target cell. The primary and charge transferred beams emerging from the target cell were alternately deflected by plates CA into a channel electron multiplier. Incident particle fluxes ranged from 2×10^4/sec for lower charge states to as low as 50/sec for +5.

The experimental system was pumped by five separate diffusion pumps, with the 15-cm pumps on either side of the target cell having liquid-nitrogen traps. Base pressures in the system were less than 1×10^{-7} Torr (1.3×10^{-5} Pa), and operating pressures were typically 2×10^{-7} Torr (2.7×10^{-5} Pa).

The use of electrostatic deflectors for charge-state selection is quite convenient for beams such as were employed here. However, some problems arise which must be recognized and accounted for. In the case of nitrogen, for example, the bulk of the ions produced by the ion source were N_2^+ ions. These molecular ions can be dissociated by collisions with background gas after the initial 90° deflection but before magnetic analysis. As a result of this dissociation, a beam of nitrogen ions having $\frac{1}{2}$ the energy of the molecular ions is produced. This slow N^+ component is magnetically analyzed at the same field as the N^{+2} beam extracted directly from the source. Since the deflection plates CS select beams of the same energy per unit charge, there is an accidental overlap between the slow N^+ and the N^{+4} beam produced by stripping the incident fast N^{+2} beam. As a result of this accidental degeneracy in the charge selection, +4 and +5 beams were obtained by extracting the weaker +3 component directly from the source and passing it through a stripper foil. Similar problems occurred for the C^{+q} and O^{+q} beams which were obtained using CO in the ion source. Because of the mass differences in the slow dissociation products formed from CO^+, they could be separated from the desired multiply charged ions by careful adjustment of the lens and charge selector. The beam charge-state purity was checked by increasing the hydrogen target thickness and scanning the voltage on deflector plates CA for spurious charge transfer components. In the worst case the beam purity was determined to be better than 95%.

Particles were detected with channel electron multipliers employing conventional pulse-counting techniques. A scan of the beam profiles of the incident and charge transferred beams produced a flat-topped response on the movable detector shown in Fig. 1, indicating complete beam collection. The efficiency of the detector for all ions and neutral particles investigated was taken to be 1. The detector cones were grounded and ungridded. Careful checks were performed to ensure the linear response of the detection system as a function of count rate over the entire range of particle energies. Identical count rates were always observed with either the fixed or the movable detector.

B. Atomic-hydrogen target

The atomic-hydrogen target was produced by thermally dissociating molecular hydrogen in an oven similar to that used by McClure.[7] The oven was formed by rolling 0.025-mm tungsten foil into a tube having a nominal diameter of 6 mm. The target cell was defined by positioning two tungsten apertures 25 mm apart inside the tube. The diameters of the entrance and exit apertures were 0.25 and 2.0 mm. The small target-cell entrance aperture also served as a beam-limiting aperture, while the large ratio of exit to entrance apertures ensured that no beam was intercepted at the exit aperture.

Hydrogen gas was admitted to the target cell through a gas handling system with which the relative gas flow to the cell could be carefully measured and controlled by determining the pressure drop ΔP across a capillary using a capacitance manometer. This technique proved most useful in providing excellent reproducibility of target gas density from run to run. As discussed below, absolute target densities were determined by normalizing our relative data to well accepted previous results of other investigators. Another feature of the gas handling system was the addition of a valve which could be used to bypass the target cell and admit the target gas flow directly into the region

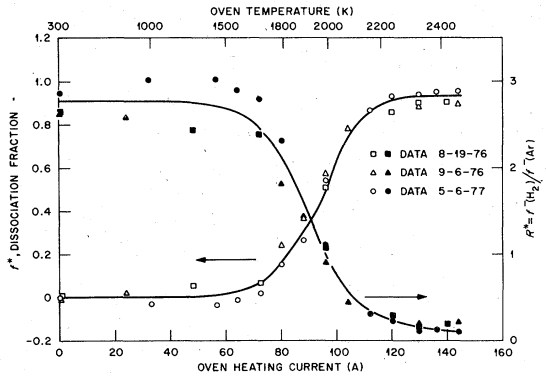

FIG. 2. The dissociation fraction f^* and the ratio R^* of double-electron-capture signals for H_2 and Ar target gases as a function of the oven heating current and temperature.

surrounding the oven tube through a comparable conductance. This "gas dump" technique allows the subtraction of counts which arise as a result of aperture scattering or from collisions with background gas.[8]

The primary consideration in using the atomic-hydrogen target is the measurement of the fraction of the molecular hydrogen dissociated in the oven. We used the well established method of observing double electron capture for protons passing through the target cell under single-collision conditions.[9] In principle, this measurement can be made using any incident ion that has a significant double-electron-capture cross section. For our purposes, a proton beam at 20 keV was selected, and the primary beam (typically 10^{-12} A) was measured with an electrometer while the H^- charge transfer component was counted. Details of the analysis are described in the Appendix. The results of our dissociation measurements are given in Fig. 2. The same tungsten target cell was used for all measurements. All the cross sections presented in the present communication were taken for a measured dissociation fraction 0.92 ± 0.03. Oven-wall temperatures were monitored with a pyrometer for each data point, and reproducibility of ± 20 K for a given heating current was observed over the duration of the experiment. Operating conditions were determined by setting the oven current to 130 A as measured using a precision current shunt and a digital voltmeter, and corresponded to a pyrometrically determined temperature of 2350 K.

Preliminary measurements revealed that the heated oven was a copious emitter of electrons as well as photons, which were detectable by the channel electron multipliers used. The electron current resulted from thermionic emission and was suppressed by floating and appropriately biasing the oven heater supply. A plate having a 3-mm aperture and the deflection plates CA were arranged to eliminate the line-of-sight path from the detectors to the oven for all except on-axis measurements of neutrals. Photon background counts were reduced in this manner to a level where reliable data could be obtained using the extremely small beam fluxes obtained during parts of the experiment.

C. Data acquisition and reduction

For all measurements involving charged product species, the particle detector was positioned off axis, and the primary and charge transferred beams were alternately deflected into the detector and counted. Corrections to the raw data were made by subtracting counts obtained in the gas dump mode. This correction was typically 10–20%, most of which was due to aperture scattering. The incident +4 and +5 beams were of such low intensity that background counts from photons from the oven were significant and had to be subtracted, thereby introducing additional statistical uncertainty of up to 10% in some cases.

In a conventional charge transfer measurement under single-collision conditions, a cross section would be obtained from the expression

$$\sigma_{ij} = \frac{N_j}{(N_i + \sum_k N_k)\,\pi}\,, \tag{1}$$

where N_i is the number of incident ions remaining after the target, N_j is the number of product ions (or atoms), the sum $\sum_k N_k$ is over all possible reaction products, and π is the effective target-density–target-cell length product (target thickness). The products arising from stripping of the incident ions were measured to be smaller than those for electron capture by factors of 10 to 100 in the energy region studied, and hence the sum in Eq. (1) was replaced by N_j with an accuracy of much better than 1%. Direct measurement of π is difficult, particularly for an atomic hydrogen target. Since reliable cross section measurements exist that could be used to normalize our relative results, we decided to obtain absolute cross sections by the following procedure.

The raw data were reduced to relative count rates using the relation

$$C_{ij} = \frac{N_j}{(N_i + N_j)\,\Delta P}\,, \tag{2}$$

where N_i and N_j are defined above, and ΔP is the pressure drop across the capillary of the gas handling system. Absolute cross sections were obtained from the relative count rates defined in Eq. (2) by determining the relation between the measured pressure drop ΔP and the actual target thickness for the target cell. For the H_2 measure-

ments, this normalization was accomplished by measuring the charge transfer signal C_{10} for the reaction $H^+ + H_2 \rightarrow H + H_2^+$ at 20 keV and comparing our result to the earlier cross-section measurements of Stier and Barnett,[10] and McClure,[7] $\sigma_{10} = 6.0\times10^{-16}$ cm^2. This gave a target-thickness calibration $\pi/\Delta P = 5.80\times10^{14}$ particles/cm^2 Torr.

For the hot atomic-hydrogen target, we must take into account the presence of undissociated molecular hydrogen in the target cell. As shown in the Appendix, $\pi^*(H)$ for the hot target is given by

$$\pi^*(H) = \frac{C_{10}^*}{\sigma_{10}(H) + \sigma_{10}(H_2)(1-f^*)/2f^*}, \quad (3)$$

where $\pi^*(H)$ is the atomic-hydrogen target thickness, C_{10}^* is the relative count rate of neutrals produced in electron transfer collisions by protons in the hot target cell, f^* is the dissociation fraction, and $\sigma_{10}(H)$ and $\sigma_{10}(H_2)$ are the single-electron charge-exchange cross sections for atomic- and molecular-hydrogen targets, respectively. Measurements of C_{10}^* were made for 20-keV protons, and the value of $\sigma_{10}(H) = 5.2\times10^{-16}$ cm^2 as independently determined by McClure[7] and Bayfield[11] was used in Eq. (3) to calculate $\pi^*(H)/\Delta P$ (2.66×10^{14} particles/cm^2 Torr).

To establish consistency in this normalization procedure, relative cross sections σ_{10} were also measured for 50- and 100-keV protons and were found to reproduce the energy dependence of previous measurements.[7,10,11] As a further check, estimates were made of the gas density in the target cell employing gas kinetic theory. Conductances were calculated for the capillary of the gas handling system and the target-cell assembly. These estimates for both hot- and cold-target conditions agree with those obtained above using the normalization procedure to within 8% for H_2 and 2% for H.

It was established in both the calibration procedure and cross-section measurements that the observed charge transfer signals were linear with ΔP. Target-cell densities were typically 3×10^{12} cm^{-3} for H and 6×10^{12} cm^{-3} for H_2, and were chosen to result in a charge transfer component which was 2% or less of the primary beam to ensure single-collision conditions.

III. UNCERTAINTIES

Table I lists estimated systematic uncertainties from various sources associated with both the target-thickness calibrations and the individual cross-section measurements. In those cases where insufficient data are available for statistical analysis, the uncertainties have been evaluated at a level which is considered roughly equivalent to the 90% confidence level on statistically derived quantities. The reproducibility of the target-thickness calibrations represents the 90% confidence limits on the values obtained on seven different determinations made at various intervals during the experiment (4 months). The uncertainty due to ion-beam impurity represents the worst possible case where some difficulties were encountered in resolving the higher-charged species from slow molecular ion dissociation contaminants (see Sec. II A). The assessment of possible effects on the cross sections due to target-gas impurity is based on the dissociation-fraction measurements as well as on measurements made with the hydrogen gas valve closed, which allow estimates of residual scattering due to gases evolved from the gas handling system. The experimentally measured dissociation fractions are sensitive to gas purity since atomic hydrogen is the only neutral species that has a zero cross section for double-electron transfer to another atom or ion. The dissociation fractions were measured as a function of temperature on three different occasions during the course of the experi-

TABLE I. Summary of systematic uncertainties.

Source	$\sigma_{ij}(H_2)$	$\sigma_{ij}(H)$
Reproducibility of target-thickness calibration (90% C.L.)	±3	±5
Measurement and reproducibility of ΔP	±2	±2
Target-gas purity (maximum effect on σ_{ij})	±6	±3
Ion-beam purity (maximum effect on σ_{ij})	±5	±5
Beam collection and counting efficiency	±2	±2
Uncertainty in f^* (maximum effect on σ_{ij})		±4
Reproducibility of temperature (maximum effect on π)	±2	±2
Quadrature sum	±9%	±9%

TABLE II. Charge transfer cross sections σ_{ij} for carbon ions incident on atomic- and molecular-hydrogen targets. Total relative uncertainties are given (see Sec. III). All cross sections are in 10^{-16} cm^2/molecule for H_2 and 10^{-16} cm^2/atom for H.

C^{+q} energy (keV)	Relative velocity (10^8 cm/s)	σ_{10}(H)	σ_{10}(H_2)	σ_{21}(H)	σ_{21}(H_2)	σ_{32}(H)	σ_{32}(H_2)	σ_{43}(H)	σ_{43}(H_2)
8.6	0.37	6.1 ± 0.7	2.0 ± 0.2						
20	0.57	8.9 ± 0.8	4.9 ± 0.5						
40	0.80			8.4 ± 0.8	13.0 ± 1.2				
50	0.90	8.3 ± 0.7	8.2 ± 2.8						
60	0.98					14.8 ± 1.4	7.9 ± 0.8		
100	1.27	5.5 ± 0.7	7.5 ± 0.7	7.5 ± 0.7	10.0 ± 0.9				
150	1.55					16.4 ± 1.5	12.4 ± 1.1		
200	1.79	4.0 ± 0.5	5.6 ± 0.5	6.9 ± 0.6	8.0 ± 0.7				
240	1.96					16.2 ± 1.5	14.1 ± 1.3		
300	2.20	3.2 ± 0.4	4.3 ± 0.4						
400	2.54	2.4 ± 0.3	3.3 ± 0.3	5.1 ± 0.5	6.4 ± 0.6	13.1 ± 1.2	13.0 ± 1.2		
500	2.84	1.7 ± 0.2	2.6 ± 0.2						
600	3.11	1.4 ± 0.2	1.9 ± 0.2	3.1 ± 0.3	4.4 ± 0.4	8.8 ± 0.8	10.3 ± 0.9	14.7 ± 2.9	14.9 ± 2.2
700	3.35		1.5 ± 0.1						
800	3.59					4.5 ± 0.5	6.5 ± 0.6		
900	3.80							6.6 ± 2.0	9.1 ± 1.3
1000	4.01					2.8 ± 0.3	4.7 ± 0.4		
1200	4.39					1.7 ± 0.2	3.1 ± 0.3	3.4 ± 0.4	5.6 ± 0.6
1350	4.66					1.2 ± 0.1	2.4 ± 0.2	1.9 ± 0.2	4.2 ± 0.5
1650	5.15							1.1 ± 0.2	2.3 ± 0.2

ments, and the listed uncertainty reflects the scatter in the various values obtained. The quadrature sums represent our assessment of total systematic uncertainties in the relative experimental measurements, but do not reflect any uncertainties in the cross sections used for normalization; the consistency in existing measurements of these cross sections at 20 keV is better than 15% for both H and H_2 targets. Statistical uncertainties in the individual measurements at 90% confidence level ranged from a few percent for the lower charge states to 20% for some of the +4 and +5 data points. The uncertainties listed in Tables II–IV represent the combination in quadrature of relative systematic uncertainties from Table I with statistical uncertainties at 90% confidence level.

The effects of metastable ions in the projectile beam on charge transfer measurements have been recently investigated.[12,13] For our σ_{32} measurements, a number of data points were acquired with N^{+3} beams obtained by direct extraction from the source, by stripping N^{+2} ions on gas, or by stripping in a thin foil. The cross sections obtained for these three measurements agreed to within the statistical uncertainties of 5–10%. For this particular case, there would appear to be either insignificant metastable contamination of the primary beam, or negligible difference in the charge transfer cross sections for metastable and ground-state ions. The latter conclusion is supported by results obtained by Dmitriev *et al.*,[12] who investigated metastable content in He-like multicharged ion beams by measuring both electro. capture and -loss cross sections for foil- and gas-stripped beams, as well as beams extracted directly from the ion source. They found that the electron-capture cross sections were relatively insensitive to mode of beam preparation, while the electron-loss cross sections varied by factors of 2 to 6, indicating significant and varying metastable content.

IV. EXPERIMENTAL RESULTS AND DISCUSSION

The results of the present measurements are shown in Figs. 3–5 and are enumerated in Tables II–IV. Some of these data have been reported previously in brief communications.[14] Prior results of other investigators are given for comparison.[15] There is agreement to within 10% with the work of Crandall *et al.*[2] for molecular-hydrogen targets. The agreement of σ_{10} for nitrogen and oxygen ions with the early work of Stebbings *et al.*[16] involving an atomic-hydrogen target is comparable, if their results are renormalized as suggested by Shah and Gilbody.[17] The original normalization by Stebbings *et al.* relied on their own earlier measurements of $H^+ + H$ charge transfer cross sections. Since more recent measurements by McClure[7] and Bayfield[11]

TABLE III. Charge transfer cross sections σ_{ij} for nitrogen ions incident on atomic- and molecular-hydrogen targets. Total relative uncertainties are given (see Sec. III). All cross sections are in 10^{-16} cm^2/molecule for H_2 and 10^{-16} cm^2/atom for H.

N^{+q} energy (keV)	Relative velocity (10^8 cm/s)	σ_{10}(H)	$\sigma_{10}(H_2)$	σ_{21}(H)	$\sigma_{21}(H_2)$	σ_{32}(H)	$\sigma_{32}(H_2)$	σ_{43}(H)	$\sigma_{43}(H_2)$	σ_{54}(H)	$\sigma_{54}(H_2)$
10	0.37	6.2 ± 0.6	6.7 ± 0.6								
20	0.52	8.2 ± 0.9	8.5 ± 0.8								
40	0.74			4.2 ± 0.4	7.9 ± 0.8						
50	0.83	7.3 ± 1.2	9.8 ± 0.9								
60	0.91					18.3 ± 1.9	9.0 ± 1.0				
66.7	0.96			5.0 ± 0.5	7.7 ± 0.7						
100	1.17	4.6 ± 0.8	7.5 ± 0.7	4.9 ± 0.5	7.0 ± 0.6	17.5 ± 1.7	10.6 ± 1.1				
150	1.44	4.6 ± 0.6	5.6 ± 0.5								
200	1.66	3.2 ± 0.4	4.9 ± 0.4	5.7 ± 0.6	6.2 ± 0.6	15.3 ± 1.8	14.7 ± 1.5				
250	1.86	2.8 ± 0.3	4.2 ± 0.4								
300	2.03	2.5 ± 0.3	3.9 ± 0.4	5.8 ± 0.6	6.3 ± 0.6	14.1 ± 1.3	15.5 ± 1.8				
400	2.35			4.9 ± 0.5	5.6 ± 0.5						
450	2.49	1.8 ± 0.2	2.9 ± 0.3								
500	2.62			3.9 ± 0.4	5.0 ± 0.5	10.3 ± 1.0	12.7 ± 1.3				
550	2.75	1.4 ± 0.2	2.1 ± 0.2								
600	2.88			3.1 ± 0.3	4.3 ± 0.4			14.3 ± 4.0	19.5 ± 2.8		
700	3.11					6.9 ± 0.8	9.4 ± 1.0				
750	3.21							12.3 ± 1.5	15.8 ± 2.4	17.3 ± 3.2	20.1 ± 2.4
900	3.52					4.2 ± 0.4	6.2 ± 0.6			14.3 ± 3.2	14.7 ± 1.9
1000	3.71							7.4 ± 1.0	10.1 ± 1.0		
1100	3.89					2.9 ± 0.4	4.6 ± 0.5			8.8 ± 1.4	11.6 ± 2.1
1200	4.07							4.7 ± 0.5	7.7 ± 0.7		
1350	4.31					1.6 ± 0.2	3.0 ± 0.3	2.7 ± 1.0	5.1 ± 0.8		
1650	4.77							2.0 ± 0.5	4.2 ± 0.5	3.8 ± 0.7	4.7 ± 1.3

TABLE IV. Charge transfer cross sections σ_{ij} for oxygen ions incident on atomic- and molecular-hydrogen targets. Total relative uncertainties are given (see Sec. III). All cross sections are in 10^{-16} cm^2/molecule for H_2 and 10^{-16} cm^2/atom for H.

O^{+q} energy (keV)	Relative velocity (10^8 cm/s)	σ_{10}(H)	$\sigma_{10}(H_2)$	σ_{21}(H)	$\sigma_{21}(H_2)$	σ_{32}(H)	$\sigma_{32}(H_2)$	σ_{43}(H)	$\sigma_{43}(H_2)$	σ_{54}(H)	$\sigma_{54}(H_2)$
11.4	0.37	4.4 ± 0.8	10.3 ± 0.9								
20	0.49	4.9 ± 0.5	11.1 ± 1.0								
40	0.69			3.0 ± 0.3	4.0 ± 0.4						
50	0.78	4.2 ± 0.4	9.4 ± 0.9								
75	0.95					21.3 ± 2.0	11.8 ± 1.1				
100	1.10	3.5 ± 0.6	6.3 ± 0.6	4.3 ± 0.4	4.9 ± 0.5						
150	1.34					18.5 ± 1.7	13.9 ± 1.4				
200	1.55	2.2 ± 0.4	4.0 ± 0.4	5.1 ± 0.5	5.1 ± 0.5						
240	1.70					16.8 ± 1.8	13.5 ± 1.4				
300	1.90	1.5 ± 0.3	3.0 ± 0.3								
400	2.20	1.2 ± 0.3	2.5 ± 0.2	5.0 ± 0.5	5.3 ± 0.5	14.7 ± 1.4	14.0 ± 1.3				
500	2.46	1.2 ± 0.2	2.0 ± 0.2								
600	2.69	0.8 ± 0.2	1.6 ± 0.1	3.3 ± 0.3	4.1 ± 0.4	10.6 ± 1.0	12.1 ± 1.1	15.1 ± 2.0	15.4 ± 1.5		
800	3.11					6.4 ± 0.6	8.4 ± 0.8	12.1 ± 1.2	14.8 ± 1.4	18.4 ± 4.0	21.2 ± 2.3
1000	3.47					4.1 ± 0.4	6.0 ± 0.5	6.9 ± 0.9	10.9 ± 1.1	16.5 ± 1.9	18.0 ± 2.0
1100	3.64									12.5 ± 1.6	16.5 ± 1.7
1200	3.80					2.6 ± 0.2	4.2 ± 0.4	5.0 ± 0.5	7.8 ± 0.8	9.6 ± 1.0	14.0 ± 1.5
1350	4.03					2.0 ± 0.2	3.4 ± 0.3				

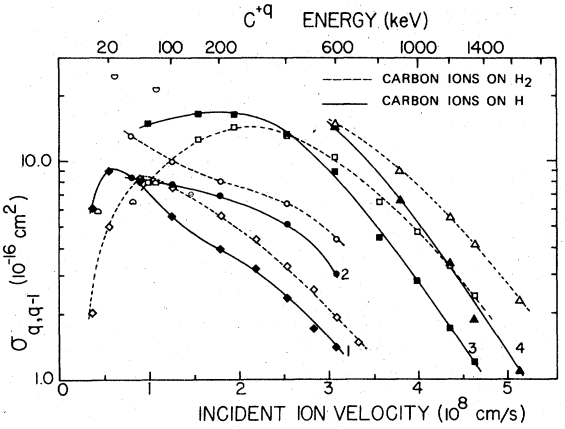

FIG. 3. Experimental electron-capture cross sections for $C^{+q}+H \rightarrow C^{+q-1}+H^+$ (solid points and curves) and for $C^{+q}+H_2 \rightarrow C^{+q-1}+H_2^+$ (open points and dashed curves). The solid curves are labeled by the incident ionic charge q. Diamonds, $q=1$; circles, $q=2$; squares, $q=3$; triangles, $q=4$. The open semicircles ⌓ are measurements of $\sigma_{32}(H_2)$ (Ref. 2); ⌔ are measurements of $\sigma_{43}(H_2)$ (Ref. 2).

suggest that this normalization results in cross sections that are approximately 30% too large, the data from Stebbings *et al.* that are shown have been reduced by 30% to reflect these more recent results.

Asymmetric charge transfer processes involving

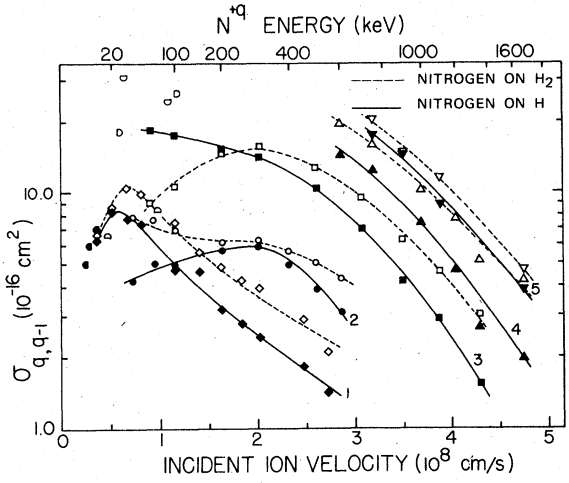

FIG. 4. Experimental electron-capture cross sections for $N^{+q}+H \rightarrow N^{+q-1}+H^+$ (solid points and curves) and for $N^{+q}+H_2 \rightarrow N^{+q-1}+H_2^+$ (open points and dashed curves). The solid curves are labeled by the incident ionic charge q. Diamonds, $q=1$; circles, $q=2$; squares, $q=3$; triangles, $q=4$; inverted triangles, $q=5$. The open semicircles ⌓, ⌔, and D are measurements of $\sigma_{32}(H_2)$, $\sigma_{43}(H_2)$, and $\sigma_{54}(H_2)$, respectively (Ref. 2). The solid semicircles ◖ are measurements of $\sigma_{10}(H)$ (Ref. 16).

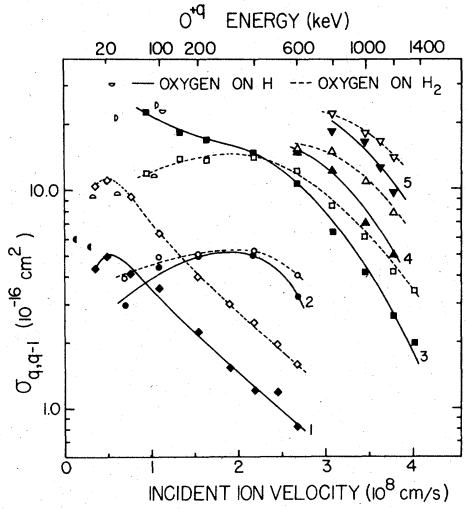

FIG. 5. Experimental electron-capture cross sections for $O^{+q}+H \rightarrow O^{+q-1}+H^+$ (solid points and curves), and for $O^{+q}+H_2 \rightarrow O^{+q-1}+H_2^+$ (open points and dashed curves). The solid curves are labeled by the incident ionic charge q. Diamonds, $q=1$; circles, $q=2$; squares, $q=3$; triangles, $q=4$; inverted triangles, $q=5$. The open semicircles ⌓, ⌔, and D are measurements of $\sigma_{32}(H_2)$, $\sigma_{43}(H_2)$, and $\sigma_{54}(H_2)$, respectively (Ref. 2). The solid semicircles ◖ are measurements of $\sigma_{10}(H)$ (Ref. 16).

singly charged projectiles have been described in terms of the adiabatic criterion. This simple treatment predicts a cross section for charge transfer which increases with increasing projectile velocity to a maximum for $v \simeq a|\Delta E|/\hbar$, where $|\Delta E|$ is the energy difference between the initial and final states of the system in the separated-atom limit and a is some internuclear separation characteristic of the dynamical collision system. Hasted and Lee have evaluated many asymmetric charge transfer reactions and from empirical considerations have chosen a value of $(7-8)\times 10^{-8}$ cm for a.[18] Rapp and Francis have applied a quasimolecular model using semiempirical orbitals and arrived at a similar criterion for the location of the peak of the charge transfer cross section.[19] At higher velocities they calculate the asymmetric cross sections to have the same energy dependence as that for symmetric charge transfer.

For multiply charged incident ions, both collision products are positively charged. As a result, the appropriate potential curves for the products are repulsive, as is indicated schematically in Fig. 6. The repulsive curves correspond to the ground state and to various excited states of the products and are shown crossing a potential curve characteristic of the initial ion-atom system. For the large internuclear separations at which charge transfer occurs, the behavior of this potential

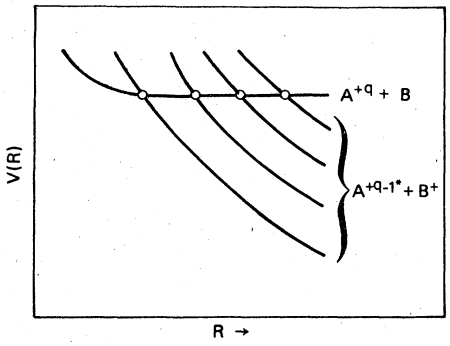

FIG. 6. Schematic representation of the potential curves of the electron-transfer reaction $A^{+q}+B \rightarrow A^{+q-1}+B^{+}$.

curve is dominated by the polarization of the target system by the incident ion.

In the case of charge transfer involving multiply charged ions, it is useful to consider a Landau-Zener formalism, as was initially done by Hasted and co-workers.[20,21] Using such a treatment, Bates and Moiseiwitsch[22] and Dalgarno[23] calculated cross sections for charge transfer between various multiply charged ions and atomic hydrogen for low-velocity collisions. More recently, Salop and Olson have applied this model to calculations of charge transfer processes between fully stripped multicharged ions and atomic hydrogen for relative velocities less than 10^8 cm/s.[24] These calculations involved modification of the Landau-Zener theory to a multicrossing system. The cross sections calculated were all greater than 10^{-15} cm^2 at a relative velocity of 10^8 cm/s. They found that the important final states of the product heavy ion were excited states having asymptotic energies some tens of eV below the initial state. These states were most likely to cross the initial states in a region where the Landau-Zener formula gives a large probability of charge transfer. Some evidence for the participation of excited states of the multiply charged product ion in these charge transfer processes appears to have been found by Isler, who recently reported the prompt appearance of Balmer lines from O^{+7} when neutral hydrogen atoms are injected into ORMAK, the Oak Ridge tokamak device.[25]

Salop and Olson further found that the velocity dependence of the cross sections weakened as the number of participating final excited states (i.e., the number of pseudocrossings) increased. The relative energy independence of our measured σ_{32} cross sections at velocities below 2×10^8 cm/s would suggest on this basis the presence of multiple exit channels for these reactions.

For velocities above 3×10^8 cm/s, the cross sections fall sharply. Presnyakov and Ulantsev have studied charge transfer between multiply charged ions ($q>10$) and atoms.[26] They assume coupling between a number of levels and calculate cross sections for transfer into various excited states. A general result of their calculation is a q^2 scaling of the cross section for incident velocities above 3×10^8 cm/s. In Fig. 7 the charge scaling of our results is shown; there is some evidence for the predicted behavior. Nikolaev *et al.* have experimentally investigated charge transfer cross sections at projectile velocities above 3×10^8 cm/s for various multiply charged ions on rare gases.[1] They find $\sigma_{q,q-1} \propto q^N$, where N increases with increasing velocity. In the case of nitrogen projectile ions, for example, they found that N increased from 1.5 to 3.0 as the relative velocity increased from 2.6 to 8.0×10^8 cm/s.

Olson and Salop have calculated cross sections for a large number of charge transfer reactions in the high-velocity region ($v>2\times10^8$ cm/s).[27] The calculations predict ionization as well as charge transfer cross sections. A classical Monte Carlo method was used which entailed numerically solving the 12 coupled Hamilton's equations of motion for a three-body system with a random distribution of initial conditions. The three bodies were the incident ion N^{+q}, the hydrogen-ion target, and the electron initially moving around the hydrogen ion. The electron distribution about the proton is described classically. Coulomb forces represent the interactions between all bodies. Since electron screening effectively reduces the binding energy of the electron relative to a fully stripped ion with $q=Z$, the charge of the partially stripped ion X^{+q} is given by an effective charge q_{eff}. The latter was determined from spectroscopic energy levels by fitting the excited levels n of the final state in

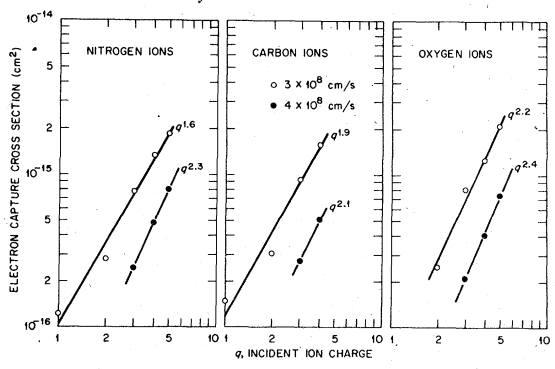

FIG. 7. Cross sections for electron capture by N^{+q}, C^{+q}, and O^{+q} incident on atomic hydrogen as a function of the incident ionic charge q; ○ for $v=3\times10^8$ cm/s; ● for $v=4\times10^8$ cm/s.

X^{+q-1} to a one-electron hydrogenic model. Figure 8 compares the results of these calculations as well as earlier absorbing-sphere calculations by Olson and Salop[28] with the present results for $\sigma_{q,q-1}$ for $O^{+q}+H$. There is good agreement between experiment and theory for higher velocities. The calculations for incident nitrogen and carbon ions agree correspondingly well. Figure 8 also shows calculations of σ_{10} by Rapp and Ortenburger,[29] and by Rapp and Francis.[19]

The results for an atomic-hydrogen target are compared with those for molecular hydrogen in Figs. 3–5. The single sharp maximum and similar shapes of all the $\sigma_{10}(H)$ and $\sigma_{10}(H_2)$ cross-section curves suggest, for this set of reactions, participation of relatively few quasimolecular potential curves in the charge transfer collision. For $\sigma_{21}(H_2)$ and $\sigma_{21}(H)$, on the other hand, multiple curve crossings seem to be occurring, since these cross sections exhibit broad maxima for all three incident ions.

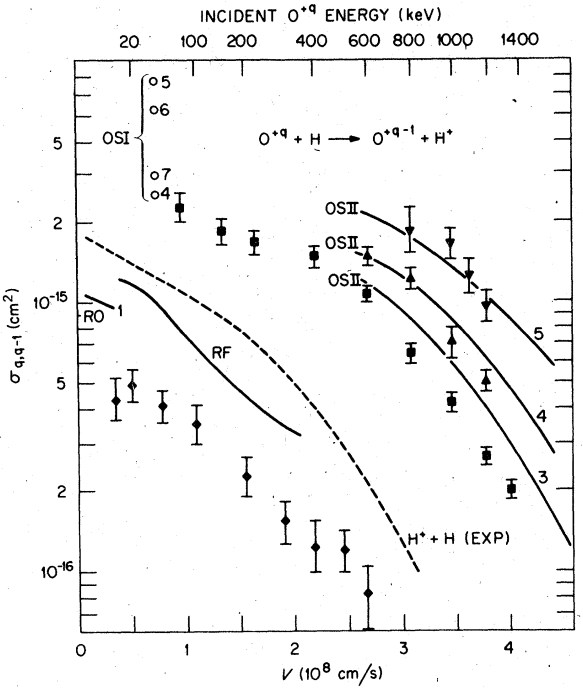

FIG. 8. Theoretical calculations of $\sigma_{q,q-1}$ for the reactions of $O^{+q}+H \rightarrow O^{+q-1}+H$. For $q=1$: RO, Rapp and Ortenburger (Ref. 29) and RF, Rapp and Francis (Ref. 19); for $q=4$, 5, 6, 7 at $v=7\times10^7$ cm/s: OSI, Olson and Salop (Ref. 28); for $q=3$, 4, and 5: OSII, Olson and Salop (Ref. 27). For comparison, results of the present measurements, as well as the measured cross section σ_{10} for $H^+ + H \rightarrow H + H^+$ (Ref. 7), are also shown. For identification of symbols, see Fig. 5. Flags on the experimental points denote the total relative uncertainties (see Sec. III).

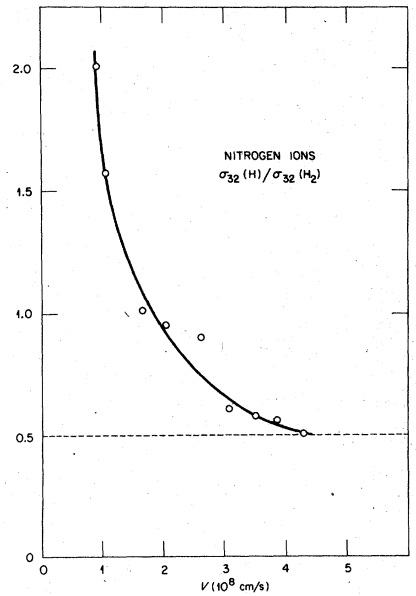

FIG. 9. The ratio of the electron-capture cross section σ_{32} for N^{+3} incident on H and H_2, respectively, as a function of relative velocity.

The measurements of σ_{32} cover the widest velocity range and serve to illustrate the differences between the atomic and molecular targets. At low velocities, the cross section $\sigma_{32}(H)$ is larger than $\sigma_{32}(H_2)$ for all three incident species. At high velocities the opposite case holds, with $\sigma_{32}(H)$ approaching $\frac{1}{2}\sigma_{32}(H_2)$. The crossover occurs for relative velocities approximately equal to the Bohr velocity. The behavior of the experimental ratio $\sigma_{32}(H_2)/\sigma_{32}(H)$ with velocity is shown in Fig. 9 for incident N^{+3} ions.

There is a lack of data for $\sigma_{43}(H_2)$ and $\sigma_{54}(H_2)$ in the velocity region between the present results and those of Crandall *et al.*[2] However, if smooth extrapolations are made between the existing data, it is obvious that no simple scaling procedure with velocity or initial ion charge will suffice to explain the low-energy behavior of these charge transfer cross sections. In terms of the general Landau-Zener model of these systems, this low-energy behavior would depend critically on the locations of the different excited states relative to the initial state, and on the locations of the crossing points.

V. SUMMARY

Our charge transfer measurements are characterized by a number of important features. The cross sections measured for the higher charge states exceed 1×10^{-15} cm^2 in most instances. For incident velocities less than approximately the

Bohr velocity, the quasimolecular nature of the collision complex becomes dominant, and significant differences appear between the cross sections for atomic and molecular targets. There seem to be no simple scaling laws that predict the low-velocity behavior of these cross sections. For higher velocities the cross sections for the higher charge states appear to depend only on the incident charge state and relative velocity, showing almost no dependence on ionic species.[30] Scaling with ion charge gives approximately a q^2 dependence; the power of q is a slowly increasing function of velocity. The significant differences in the cross sections determined for atomic and molecular hydrogen cast doubt on any estimates of cross sections for atomic targets made by scaling results for molecular targets. There is some indication, however, that for the higher velocities studied here the cross-section ratio for atomic and molecular targets is approaching a constant factor of 0.5.

For velocities below the Bohr velocity, a qualitative understanding of the various experimental cross sections would seem to be found in the Landau-Zener formalism. The scaling observed for higher velocities is not inconsistent with that predicted by existing theoretical treatments of charge transfer. The classical Monte Carlo calculations of Olson and Salop are particularly interesting because the good agreement with the present charge transfer data would lend credence to their calculated ionization cross sections for which no experimental results exist at present.

VI. ACKNOWLEDGMENTS

The authors are grateful to C. F. Barnett and D. H. Crandall for proposing the experiments, and for invaluable assistance and suggestions. In addition, we wish to acknowledge helpful discussions of theoretical considerations with R. E. Olson. We are indebted to G. W. McClure for providing design details of the hydrogen oven, and to J. A. Ray for assistance with apparatus. We thank P. Hvelplund for pointing out a sign error in Eq. (7) of Ref. 31. Oak Ridge National Laboratory is operated by Union Carbide Corporation for U. S. Department of Energy.

APPENDIX

In our experiments the fraction of dissociated hydrogen present inside the hot target cell was determined by using double electron transfer, a technique originally developed by Lockwood *et al.*[9] The treatment below is essentially that of Bayfield.[31]

If a 20-keV beam of protons (as used in the present measurements) is allowed to pass through the hydrogen target cell, a certain fraction will undergo double charge transfer under single-collision conditions. This fraction will drop as the target cell is heated due to the dissociation of H_2 and changes in cell conductance.

If similar measurements are made using argon in the target cell, changes due to cell conductance may be cancelled out by taking suitable ratios of hydrogen and argon measurements.

Ignoring double-scattering terms (justifiable for the present measurements), Bayfield has shown that the ratio of the fraction of the beam converted for hot- and cold-target conditions is

$$\frac{F^*_{-1}(\mathrm{H},\mathrm{H}_2)}{F_{-1}(\mathrm{H}_2)} = \left(\frac{T}{T^*}\right)^{1/2}\left(\frac{\pi^*(\mathrm{H}_2)}{\pi^*(\mathrm{H}_2)+\pi^*(\mathrm{H})/\sqrt{2}}\right), \tag{A1}$$

where * indicates the hot cell and π is the target thickness. Similarly, for an argon target,

$$\frac{F^*_{-1}(\mathrm{Ar})}{F_{-1}(\mathrm{Ar})} = \left(\frac{T}{T^*}\right)^{1/2}. \tag{A2}$$

If one defines $R = F_{-1}(\mathrm{H}_2)/F_{-1}(\mathrm{Ar})$, and $R^* = F^*_{-1}(\mathrm{H}_2)/F^*_{-1}(\mathrm{Ar})$, simple algebra leads to an expression for the dissociation fraction f^* as

$$f^* = \frac{R/R^* - 1}{R/R^* + \sqrt{2} - 1}. \tag{A3}$$

Figure 2 of the main text was obtained from measurements of the appropriate quantities defined above.

Because of the presence of undissociated H_2 in the target cell, a correction must be applied to the hot-cell data. The dissociation fraction can be written as

$$f^* = \frac{\pi^*(\mathrm{H})}{2\pi^*(\mathrm{H}_2)+\pi^*(\mathrm{H})}. \tag{A4}$$

Rearranging, one obtains

$$\pi^*(\mathrm{H}_2) = \frac{1-f^*}{2f^*}\pi^*(\mathrm{H}). \tag{A5}$$

The fraction of incident beam particles undergoing charge transfer is given by

$$C^*_{ij} = \sigma_{ij}(\mathrm{H}_2)\,\pi^*(\mathrm{H}_2) + \sigma_{ij}(\mathrm{H})\,\pi^*(\mathrm{H})$$

or

$$\sigma_{ij}(\mathrm{H}) = \frac{C^*_{ij}}{\pi^*(\mathrm{H})} - \frac{1-f^*}{2f^*}\sigma_{ij}(\mathrm{H}_2).$$

If we measure f^*, C^*_{ij} and $\sigma_{ij}(\mathrm{H}_2)$, then $\pi^*(\mathrm{H})$ can be written as

$$\pi^*(\mathrm{H}) = \frac{C^*_{ij}}{\sigma_{ij}(\mathrm{H}) + \sigma_{ij}(\mathrm{H}_2)(1-f^*)/2f^*}, \tag{A6}$$

which gives Eq. (3) of the main text.

[1]V. S. Nikolaev, I. S. Dimitriev, L. N. Fateeva, and Ya. A. Teplova, Zh. Eksp. Teor. Fiz. 40, 989 (1961) [Sov. Phys.-JETP 13, 695 (1961)].
[2]D. H. Crandall, M. L. Mallory, and D. C. Kocher, Phys. Rev. A 15, 61 (1977).
[3]D. H. Crandall, in *Proceedings of the Fourth Conference on the Scientific and Industrial Applications of Small Accelerators* (North Texas State University, 1976), edited by J. L. Duggan and J. A. Martin. Available from IEEE Service Center, 445 Hoes Lane, Piscataway, N.J. 08854.
[4]J. T. Hogan and H. C. Howe, J. Nucl. Mater. 63, 151 (1976).
[5]D. F. Gallaher and L. Wilets, Phys. Rev. 169, 139 (1968).
[6]R. E. Olson, F. T. Smith, and E. Bauer, Appl. Opt. 10, 1848 (1971).
[7]G. W. McClure, Phys. Rev. 148, 47 (1966).
[8]J. E. Bayfield, Phys. Rev. 182, 115 (1969).
[9]G. J. Lockwood, H. F. Helbig, and E. Everhart, J. Chem. Phys. 41, 3820 (1964).
[10]P. M. Stier and C. F. Barnett, Phys. Rev. 103, 896 (1956).
[11]J. E. Bayfield, Phys. Rev. 185, 105 (1969).
[12]I. S. Dmitriev, V. S. Nikolaev, Yu. A. Tashaev, and Ya. A. Teplova, Zh. Eksp. Teor. Fiz. 67, 2047 (1974) [Sov. Phys.-JETP 40, 1017 (1975)].
[13]A. Müller, H. Klinger, and E. Salzborn, J. Phys. B 9, 291 (1976).
[14]R. A. Phaneuf and R. H. McKnight, Bull. Am. Phys. Soc. 21, 1266 (1976); R. A. Phaneuf, F. W. Meyer, R. H. McKnight, R. E. Olson, and A. Salop, J. Phys. B 10, L425 (1977).
[15]The results of Bayfield *et al.* [J. E. Bayfield, P. M. Koch, L. D. Gardner, I. A. Sellin, D. J. Pegg, R. S. Peterson, and D. H. Crandall, in *Abstracts of the Fifth International Conference on Atomic Physics, Berkeley, 1976*, edited by R. Marrus, M. H. Prior, and H. A. Shugart (University of California, Berkeley, 1976), p. 126] are considered preliminary and are not included in Figures 3, 4, and 5.
[16]R. F. Stebbings, W. L. Fite, and D. G. Hummer, J. Chem. Phys. 33, 1226 (1966).
[17]M. B. Shah and H. B. Gilbody, J. Phys. B 7, 630 (1974).
[18]J. B. Hasted and A. R. Lee, Proc. Phys. Soc. Lond. 79, 702 (1962).
[19]D. Rapp and W. E. Francis, J. Chem. Phys. 37, 2631 (1962).
[20]J. B. Hasted and A. Y. J. Chong, Proc. Phys. Soc. Lond. 80, 441 (1962).
[21]J. B. Hasted and M. Hussain, Proc. Phys. Soc. Lond. 83, 911 (1964).
[22]D. R. Bates and B. L. Moiseiwitsch, Proc. Phys. Soc. Lond. A 68, 805 (1954).
[23]A. Dalgarno, Proc. Phys. Soc. Lond. A 67, 1010 (1954).
[24]A. Salop and R. E. Olson, Phys. Rev. A 13, 1312 (1976).
[25]R. C. Isler, Phys. Rev. Lett. 38, 1359 (1977).
[26]L. P. Presnyakov and A. D. Ulantsev, Sov. J. Quant. Electron. 4, 1320 (1975).
[27]R. E. Olson and A. Salop, Phys. Rev. A 16, 531 (1977).
[28]R. E. Olson and A. Salop, Phys. Rev. A 14, 579 (1976).
[29]D. Rapp and I. B. Ortenburger, J. Chem. Phys. 33, 1230 (1960).
[30]More recent measurements of cross sections for charge exchange between Si^{+q} ions and atomic and molecular hydrogen further support these conclusions [H. J. Kim, F. W. Meyer, R. A. Phaneuf, and P. H. Stelson, Phys. Rev. A (to be published)].
[31]J. E. Bayfield, Rev. Sci. Instrum. 40, 869 (1969).